



Published
July 17, 2000

Thin Solid Films 370 (2000) 18–29

*thin
solid
films*

www.elsevier.com/locate/tsf

Sputter deposition of NiTi thin film shape memory alloy using a heated target

Ken K. Ho, Gregory P. Carman*

Mechanical and Aerospace Engineering, University of California, Los Angeles, 38-137m Engineering IV, 420 Westwood Plaza, Los Angeles, CA 90095-1597, USA

Received 11 March 1999; received in revised form 22 March 2000; accepted 23 March 2000

Abstract

In this paper we present a novel method for depositing NiTi thin film by DC sputtering. The film has transformation temperatures very close to that of the target. The new process involves heating the target and does not require compositional modification of the NiTi target. Results from X-ray diffraction, differential scanning calorimeter, four-point probe, Rutherford backscattering, and transmission electron microscopy are presented. These results indicate that compositional modification can be produced by varying the target temperature. Films produced from hot targets have compositions similar to the target while films produced from cold targets were Ti deficient. Films that were produced by gradual heating of the target have compositional gradation through the film thickness. The graded films exhibit the two-way shape memory effect. © 2000 Elsevier Science S.A. All rights reserved.

Keywords: Deposition process; NiTi; Shape memory alloy; Sputtering

1. Introduction

NiTi is a shape memory alloy (SMA) that is capable of recovering strains on the order of 10%. This effect which is termed the shape memory effect occurs when the material undergoes a phase transformation from the low temperature martensite phase to the high temperature austenite phase. In the martensite phase deformation of the material is accommodated by preferential alignment of variants, i.e. different twinning planes detwin and align to accommodate the deformation. Unlike permanent deformations associated with dislocations, deformations due to detwinning are fully recoverable when heated to the austenite phase. The shape memory response is a one way effect, that is, the material recovers its original shape after heating to the austenite phase but does not revert back to its deformed state when cooled. In order to achieve two-way actuation, a biasing force such as a spring is necessary to deform the material when in the martensite phase.

Thin film NiTi is well suited for microactuation because of its large energy density (1 J/g) and large displacement (10% strain). Also the frequency responses of NiTi is

substantially improved at the microscale. Frequencies of several hundred Hertz can be achieved [1]. Specifically, with a smaller mass and larger surface to volume ratio, heat transfer is substantially increased, power requirements are lowered while retaining large actuation strains and stresses. While NiTi is a promising actuator, difficulties with processing this film have impeded wide spread use of the material.

The first work to incorporate thin film NiTi with a micro-machining process was done by Walker et al. in 1990 [2]. However, their films were amorphous as deposited. In 1990 Bush and Johnson at the TiNi Alloy Company showed the first definitive evidence of the SME (shape memory effect) in NiTi films [3]. Using a DC magnetron sputtering system and a single near equiatomic NiTi target, the as-deposited film was shown by X-ray diffraction (XRD) to be amorphous. After vacuum annealing the film exhibited the SME, although transformation temperatures were 100°C lower than the target material.

NiTi films with transformation temperatures above room temperature are difficult to manufacture. Sputtering processes typically produce films with reduced transformation temperatures (i.e. below room temperature), prohibiting its use as a practical actuator material. The reason for this is that a shift of as little as 1 at.% can reduce transformation

* Corresponding author. Tel.: +1-310-825-6030; fax: +1-310-206-2302.

E-mail addresses: kenh@seas.ucla.edu (K.K. Ho), carman@seas.ucla.edu (G.P. Carman).

temperatures by 100°C [4]. Rutherford backscattering (RBS) results presented in this paper show that deposited films deviate by up to 2 at.% in Ti. Shifts occur because titanium reacts fairly easily resulting in oxide formations, and because the angular flux distribution is different for Ni and Ti. Because of these two factors, sputter deposited films typically show a slight deficiency in titanium from the target material.

Researchers compensated for titanium deficiency, by placing additional Ti on top of the target thereby effectively altering the composition of the target. Miyazaki et al. [5] compensated for the titanium loss by placing titanium plates on top of the alloy target; Wolf et al. [6] and Gyobu et al. [7] similarly compensated with titanium foils. Quandt et al. uses a Ti-rich (54 at.% Ti) target to compensate [8]. To date, these are the only methods known by the authors of producing NiTi films with transformation temperatures above room temperatures from a single target. The other method of compensating for the titanium loss is to use a multigun cosputtering system. For example, Kruevitch et al. used a DC magnetron system to sputter from individually powered Ni, Ti, and Cu targets [9].

An additional issue in using thin film SMA is that depos-

ited films exhibit the one-way shape memory effect only. To achieve the two-way effect a biasing force is required to reshape the NiTi after it cools to the martensite phase. Kuriyashiki introduced this biasing force by tailoring precipitates in his NiTi foils (not sputtered films) such that there were compressive and tensile stresses on opposite sides of his foil [10,11]. This process requires complicated heat treatments and the stability of these precipitates after numerous thermal cycles are not known. Other SMA MEMS (microelectromechanical systems) devices rely on mechanical design to produce the two-way effect rather than material design.

There has been a large interest in using thin film SMA in MEMS devices. This has motivated studies on deposition, heat treatments, and thermomechanical characterization [12–16] but only a few actual microdevices have been fabricated. Some devices include a microvalve from the TiNi Alloy Co., which closes using a bias mass [17]. Kruevitch et al. fabricated a 900- μm long, 380- μm wide, and 200- μm tall microgripper from 5- μm thick NiTi–Cu film, as well as a functioning microvalve [9]. Benard et al. fabricated a micropump from NiTi film using two designs: polyimide as the biased actuator in one and a complementary NiTi

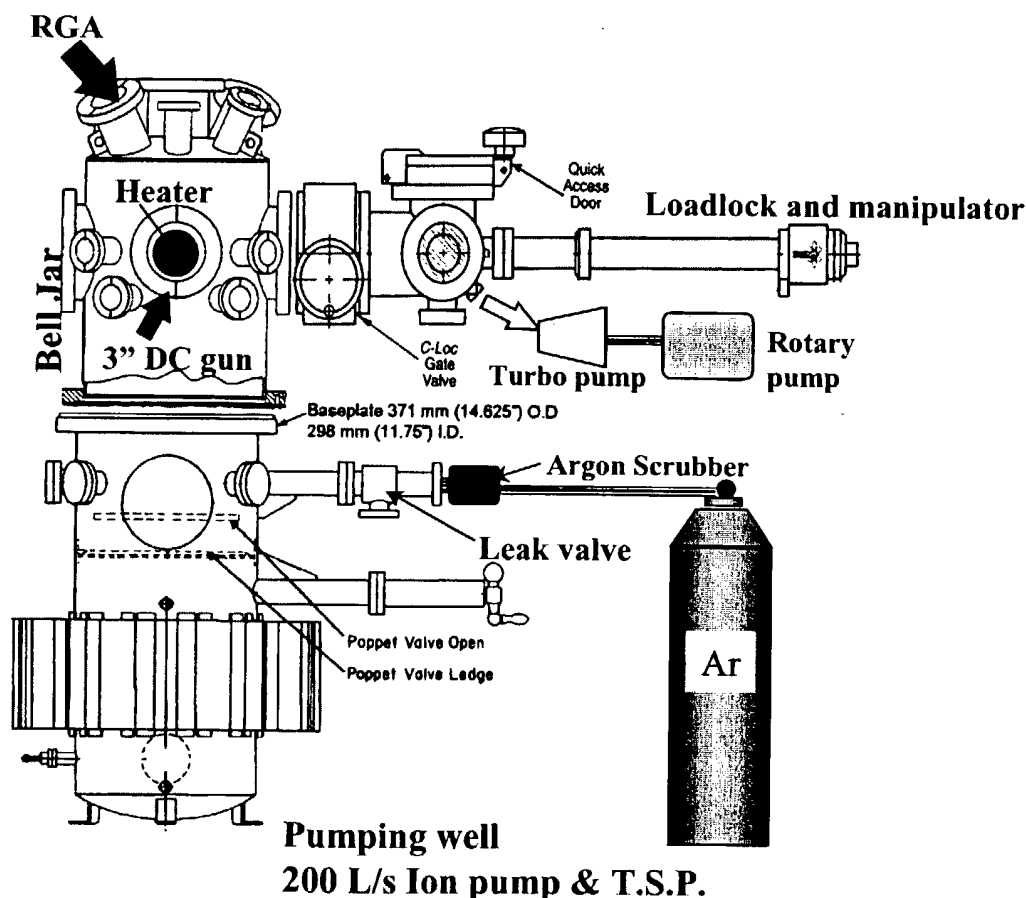


Fig. 1. Schematic and picture of UHV sputtering system for thin film NiTi.

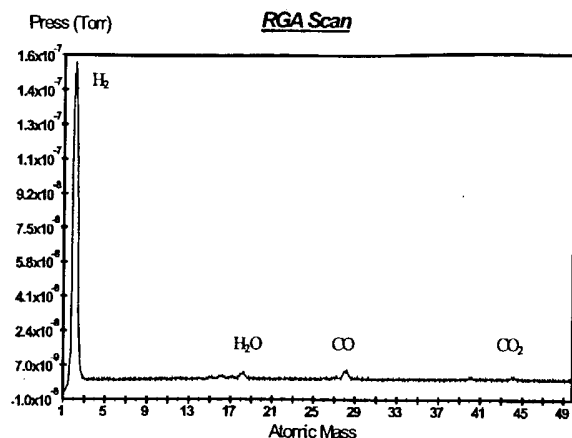


Fig. 2. Residual gases in the chamber prior to sputtering.

actuator in the other [18]. Kuribayashi et al. [11] used NiTi films to actuate a microrobotic manipulator. While the potential applications for SMA MEMS are large, the difficulties with fabricating quality material and achieving the two-way effect is preventing wide spread use of this actuator material.

In our process, a near equal atomic NiTi target is sputtered to produce quality material without compositional modification. Heating the target produces films with transformation temperatures similar to the target. When cooled the target produces deposited films that have transformation temperatures substantially lower (i.e. over 100°C) than that of the target. When the target is gradually heated compositional variation through the thickness are observed, resulting in the two-way SME. The difference in transformation temperature is attributed to compositional modification as determined by RBS measurements.

2. Experimental setup

The NiTi films presented in this paper were deposited using a dedicated sputtering system built at UCLA. A picture and schematic of the system is shown in Fig. 1. The system is UHV (ultra-high vacuum) compatible with a loadlock to decrease pump down time as well as minimize exposure to contaminants. A Stanford Research Systems RGA (residual gas analyzer) is present to monitor contamination levels, particularly water and carbon dioxide pres-

Table 1
Mean free path at varying pressures

Pressure (Torr)	Mean free path (cm)
1×10^{-6}	0.07
1×10^{-7}	0.7
5×10^{-8}	1.4
1×10^{-8}	7.0
1×10^{-9}	70

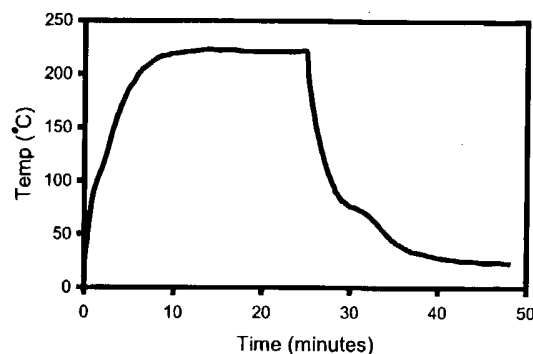


Fig. 3. Temperature profile of target when cooled.

ures, prior to sputtering. An argon scrubber is present to further clean the 99.999% purity argon gas used for the sputtering process. Sputtering is done with a 3-inch DC magnetron gun from US Thin Film Products Inc. An in situ heater with rotation capability is used to crystallize the films. The target was cut from a 3-inch diameter boule of near equiatomic NiTi purchased from Special Metals.

Prior to each run residual gas measurement were taken with the RGA to ensure a minimal amount of contamination. Initial RGA scans prior to bake-out of the vacuum system, indicate that H_2 , H_2O , CO_2 and CO were the primary gases in the system. Because of the highly reactive nature of Ti these gases can deplete the amount of Ti reaching the substrate. For this reason H_2O , CO_2 and CO gases were kept below 10^{-8} Torr (Fig. 2) for all sputtering runs. The H_2 gas had values above 10^{-8} Torr but does not react with Ti as readily and is assumed to be negligible for this discussion.

Unless otherwise noted, films were deposited using the following parameters: base pressures $< 5 \times 10^{-8}$ Torr, $P_{Ar} = 2.0$ mTorr, target substrate distance = 4.0 cm, and power = 300 W. The as-deposited films were initially amorphous and were crystallized by heating to 500°C for 10 min in situ prior to removal from the sputtering system. Deposition rates at these conditions were approximately 225 nm/min as determined from film thickness measurements using a profilometer.

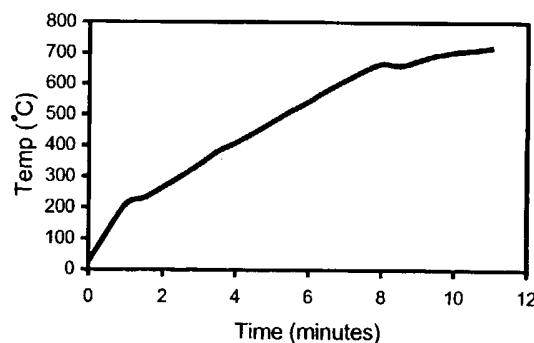


Fig. 4. Temperature profile of target when hot.

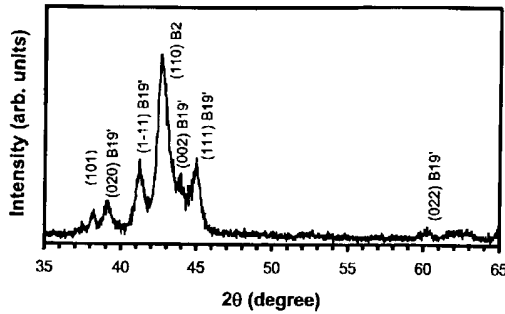


Fig. 5. XRD pattern of the NiTi target.

The mean free path for molecular collision is given by the following equation [19]

$$\lambda = \frac{kT}{\sqrt{2}P\pi\sigma^2} \quad (1)$$

where k is the Boltzmann constant, T absolute temperature, P pressure, σ molecular diameter which is roughly 10^{-8} cm for gases. Table 1 lists the mean free path calculated from Eq. (1), at different pressures. The H_2O , CO_2 and CO gas pressures prior to sputtering are below 10^{-8} Torr, which corresponds to a mean free path of >7 cm. Thus with a target substrate distance of 4.0 cm there is negligible molecular interaction to form Ti-oxides. Also, since Ti does not react appreciably with H_2 and Ar, there should be negligible Ti loss due to gettering effects as the material is sputtered. However, by slightly increasing the pressure of these gases to 5×10^{-8} Torr, mean free path reduces to 1.4 cm. Now molecular collisions between Ti and the gases would cause Ti depletion.

In this study we focus on three fabrication processes, as defined by different target temperatures. The first process uses a cool target (C samples). The target is properly cooled and has good thermal contact with the copper chill block. The target temperature, as measured using a thermocouple, stabilizes at 225°C during sputtering (Fig. 3). The second process (sample T) modifies the target temperature during sputtering such that temperatures are ramped up to $>700^\circ\text{C}$ (Fig. 4). The target transitions from a low temperature value to a high temperature value during sputtering. The higher

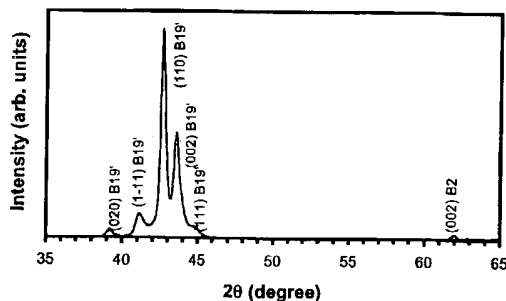


Fig. 6. XRD pattern of film sputtered from a heated target (T sample).

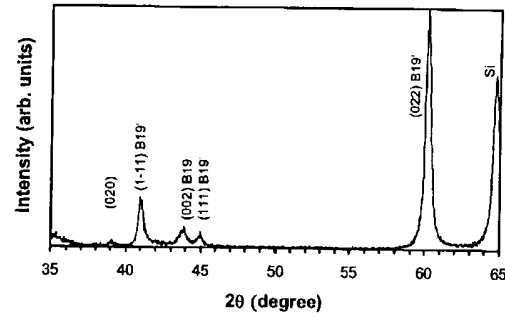


Fig. 7. XRD pattern of film sputtered from a hot target (H sample).

temperature is achieved by reducing or eliminating the thermal paste thereby producing a poor thermal contact between the target and the copper chill block. The third process (sample H) uses a hot target temperature $>400^\circ\text{C}$. This is achieved by shielding the substrate during the initial 4 minutes, then exposing the substrate when the target temperature is $>400^\circ\text{C}$.

The thickness of the C and T films, using a profilometer, are found to be approximately 2.5 μm thick. The H sample is produced by shielding the substrate during the first half of the sputtering run, then removing the shield during the last half of the sputtering run when the target temperature is $>400^\circ\text{C}$. Therefore the H sample is only 0.9 μm thick.

3. Results

Materials characterization on the three sample films are done to determine their crystalline phase, transformation temperatures and atomic composition. XRD, differential scanning calorimeter (DSC), four-point probe, RBS, and transmission electron microscopy (TEM) techniques were employed for this end.

3.1. X-Ray diffraction

XRD was performed on sputtered films attached to silicon in order to determine the NiTi film's crystalline phase. As a reference the XRD plot of the target is given in Fig. 5. XRD

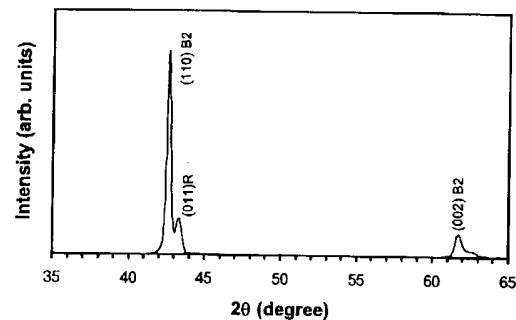


Fig. 8. XRD pattern of film sputtered from a cold target indicating an austenitic phase at 25°C.

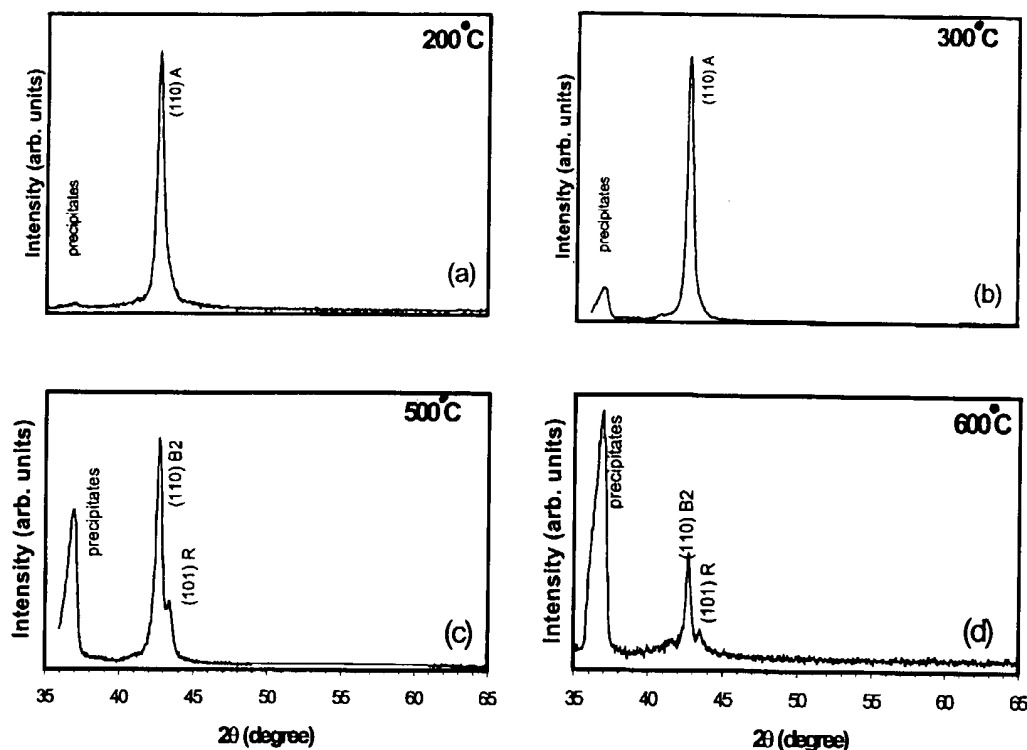


Fig. 9. XRD of films sputtered with a cold target and substrate heating. The extra diffraction peak at $2\theta = 37^\circ$ grows with increasing substrate temperature corresponding to possible precipitates.

on the T sample (Fig. 6) showed diffraction patterns similar to that of the bulk target with peaks at $2\theta = (39.2, 41.3, 43.9, 44.9^\circ)$, indexed as (020), (1–11), (110), (002), and (111) planes, respectively. This verified that the T sample has the B19' martensitic structure. In addition the T sample shows peaks at $2\theta = 42.9$ and 61.9° which are indexed as the (110) and (200) planes of the B2 austenite structure. This may suggest that the T sample has B2 austenite present.

XRD results from the H sample indicated that it was martensitic with 2θ peaks attributed to the B19' martensitic structure (Fig. 7). In contrast to the T sample, the results for the H sample did not show any peaks at $2\theta = 42.9$ and 61.9° , indicative of austenite. This indicates that the H sample consists of only the B19' phase whereas the T sample is multiphase, consisting of B2 and B19' phases. The large intensity peaks at $2\theta = 60.3$ and 64.8° are indexed as the (022) plane of the B19' structure and the silicon substrate, respectively. The silicon peak shows up in this H sample because the film is thinner than the other samples. XRD of the C sample showed peaks at $2\theta = (42.8, 43.2, 61.9^\circ)$ which correspond to the B2(110), rhombohedral (011), and B2(200) planes (Fig. 8). This implies that the crystal structure is austenite with some slight straining producing the rhombohedral phase.

To determine the influence of substrate heating, samples were deposited on a hot substrate while keeping the target cold. XRD of these samples are given in Fig. 9. The films

were deposited on a hot substrate at four different temperatures: 200, 300, 500, and 600°C and subsequently annealed at 500°C for 10 min after deposition to ensure that the films were crystallized. XRD confirm that all films are austenite at room temperatures. At the 500 and 600°C substrate temperatures the R phase begins to appear. An extra peak in the XRD at $2\theta = 37.0^\circ$ begins showing up in samples produced with 300°C substrate temperatures and grows with increasing substrate temperatures (compare Fig. 9a–d). This peak may be due to silicide formation near the film–substrate interface. Therefore, substrate heating does not produce martensitic films but rather promotes precipitate growth. Precipitates observed in TEM images will be discussed later.

3.2. Transformation temperatures

After verifying the crystal phases of the sputtered films at room temperature, the transformation temperatures of the films and target were measured, first with DSC then with four-point probe resistance. A DSC result for the C sample is given in Fig. 10. DSC results for the T sample are shown along with results for the target material (Fig. 11). DSC results for the H sample are not available because of insufficient film mass to produce accurate results. Table 2 summarizes the DSC results. Both C and T samples show a peak that is broad and short during the exothermic A to M

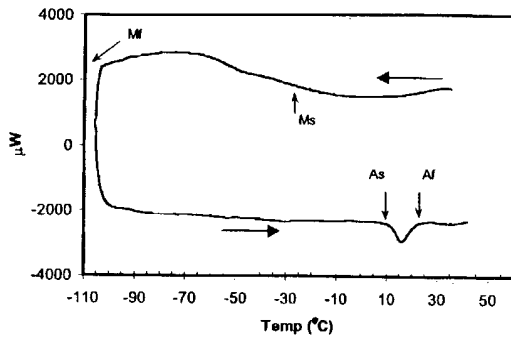


Fig. 10. DSC of a film deposited from a cold target (C sample).

transformation. This is probably due to the nonuniformity of the films, either through the thickness or radially, such that transformation is occurring over a broader temperature region. The DSC curve of the target material in contrast has transformation points that are more distinct, typical of a material with more uniform phases. Data indicates that T sample films have transformation temperatures nearly identical to that of the target material. However, when reviewing data for the C sample a distinct difference is noted. The C film has transformation temperatures 75°C below the target value. For the C film, the A_s temperature is slightly below room temperature, a property that would be representative of a superelastic material.

Four-point probe resistivity measurement was also used to measure the transformation temperatures. The four-point probe method is nondestructive and requires very small material samples. This permits measurement of transformation temperatures at different locations on the wafer to analyze the uniformity of the sputtered film. The current paper did not pursue this issue further, but chose to sample only the transformation temperatures at the center of each wafer. The resistance change versus change in temperature from the four-point probe is plotted in Fig. 12 for the target, T sample and H sample, respectively. Transformation temperatures for the C sample are unavailable because the

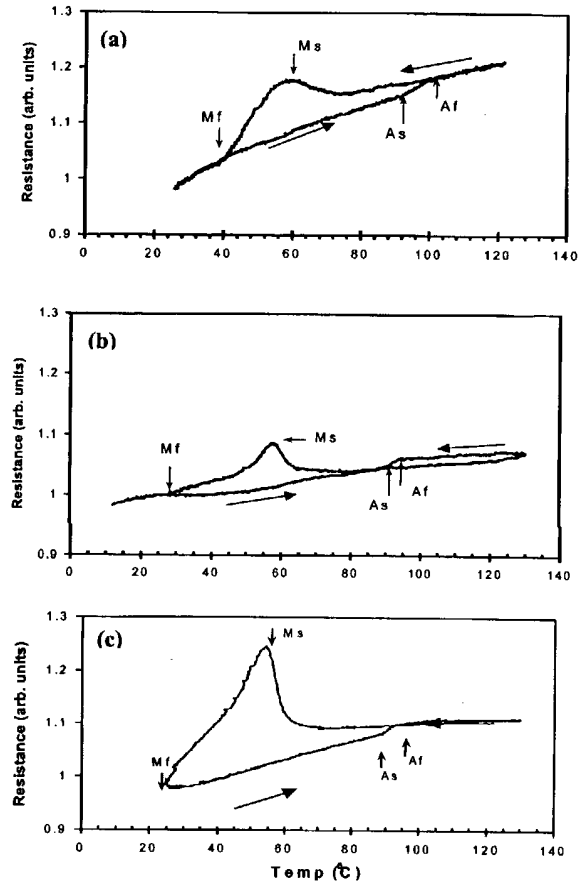


Fig. 12. Four-point probe measurement of transformation temperature of the (a) target, (b) T sample, and (c) H sample.

environmental chamber could not control temperatures accurately at below -50°C . The transformation temperatures as measured from four-point probe are summarized in Table 3. These results are consistent with those obtained from DSC, except for the A_s values. We do not attribute this difference to measurement errors as the A_s value was consistently 20°C above the DSC values. Differences in transformation temperatures measured by different approaches is a phenomena that is common in this material system.

Resistivity of the bulk target and the film samples were measured with the four point probe at room temperature. The resistivity for a bulk material and a thin film are given by the following equations, respectively

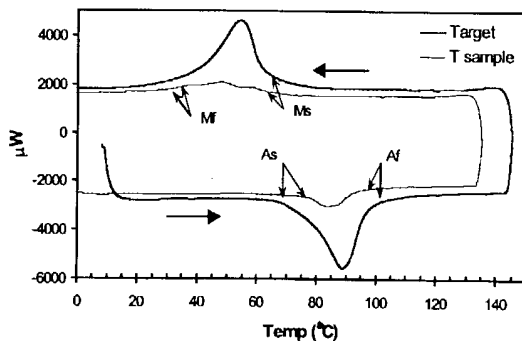


Fig. 11. DSC of a film deposited from a hot target (T sample) vs. DSC of the target.

Table 2
DSC results ($^{\circ}\text{C}$)

Sample	A_s	A_f	M_s	M_f
Target (from manufacturer)	70	100	65	35
T sample (heated target)	75	95	60	30
C sample (cold target)	10	25	-25	< -100

Table 3
Four-point probe results (°C)

Sample	A_s	A_f	M_s	M_f
Target (from manufacturer)	90	100	60	40
T sample (heated target)	90	95	55	25
H sample	90	95	55	25

$$\rho = 2\pi s \left(\frac{V}{I} \right) \quad (2)$$

$$\rho = \frac{\pi t}{\ln 2} \left(\frac{V}{I} \right) \quad (3)$$

where V is voltage, I current, s probe spacing, and t film thickness. The resistivity of the target was found to be 65 $\mu\Omega$ cm at 25°C. Resistivity for the C sample, T sample and H sample at 25°C were 93, 86, and 75 Ω cm, respectively.

Table 4
RBS results

Sample	Ni (at.%)	Ti (at.%)	Ni/Ti ratio
C sample	50.8	49.2	1.03
T sample	49.5	50.5	0.98
H sample	49.2	50.8	0.969
Target	48.2	51.8	0.931

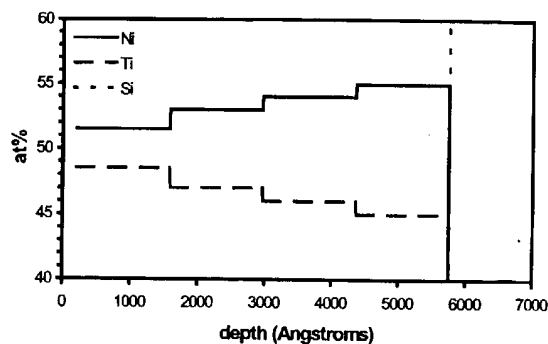


Fig. 13. RBS of sputtered film showing the compositional gradation through thickness of the film.

3.3. Compositional analysis

Compositional analysis of the target and sputtered films were done with RBS. Samples were taken from the center of each wafer. RBS is reported to be accurate to within 0.5 at.%. Results are summarized in Table 4. The composition of the target was 51.8 at.% Ti:Ni, the T sample composition was 50.5 at.% Ti, and the C sample had a composition of 49.2 at.% Ti. The H sample had a composition slightly closer to that of the target than the T sample 50.8 at.% Ti. Assuming that temperature influences Ti composition, this would be expected as the H sample was deposited from a target that was always above 450°C whereas the target temperature was ramped up from 25°C for the T sample.

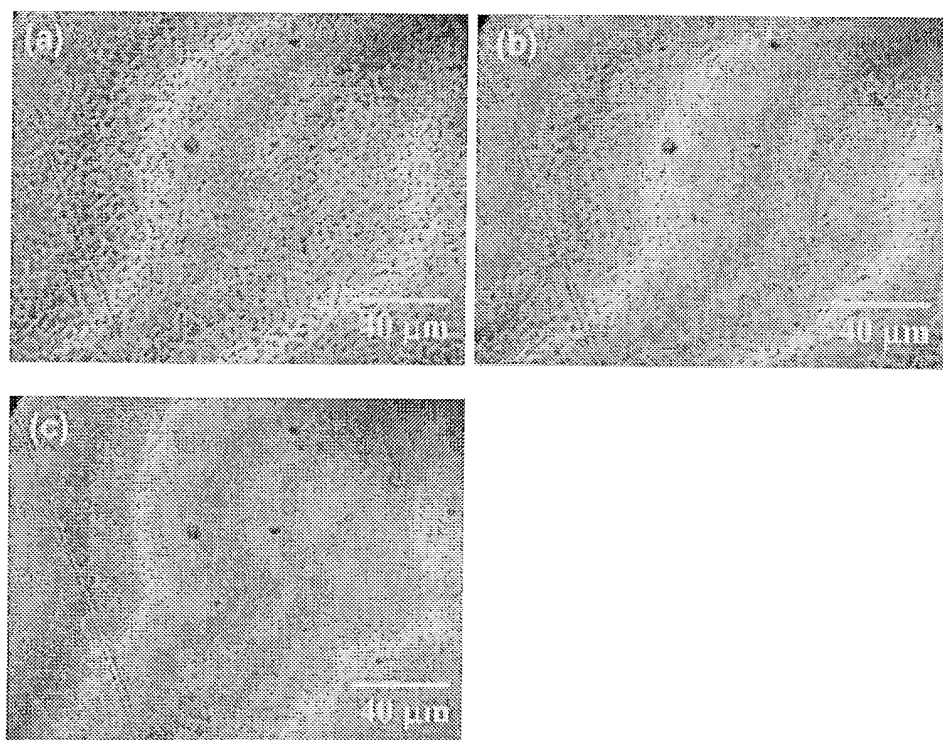


Fig. 14. Optical micrographs of martensitic platelets at (a) 25, (b) 60, and (c) 80°C.

We believe these results confirm our assumption that heating the target alters the composition of the deposited films. In this case the heated target produced films with composition very near that of the target.

As mentioned in Section 2, T samples were sputtered at temperatures transitioning from room temperature up to 700°C. As the target heats up, the film produced should have a compositional gradation through its thickness. RBS

can give composition through the thickness of a film if the film is sufficiently thin, such that the RBS signal penetrates through the film and detects the substrate reference ($<1\text{ }\mu\text{m}$). To obtain films thin enough for observing compositional variation through the thickness, the T sample film was divided into thinner sections by sputtering for 4 min then rotating the substrate to sputter the remaining 6 min on a new location. The initial 4 min of sputtering, which corre-

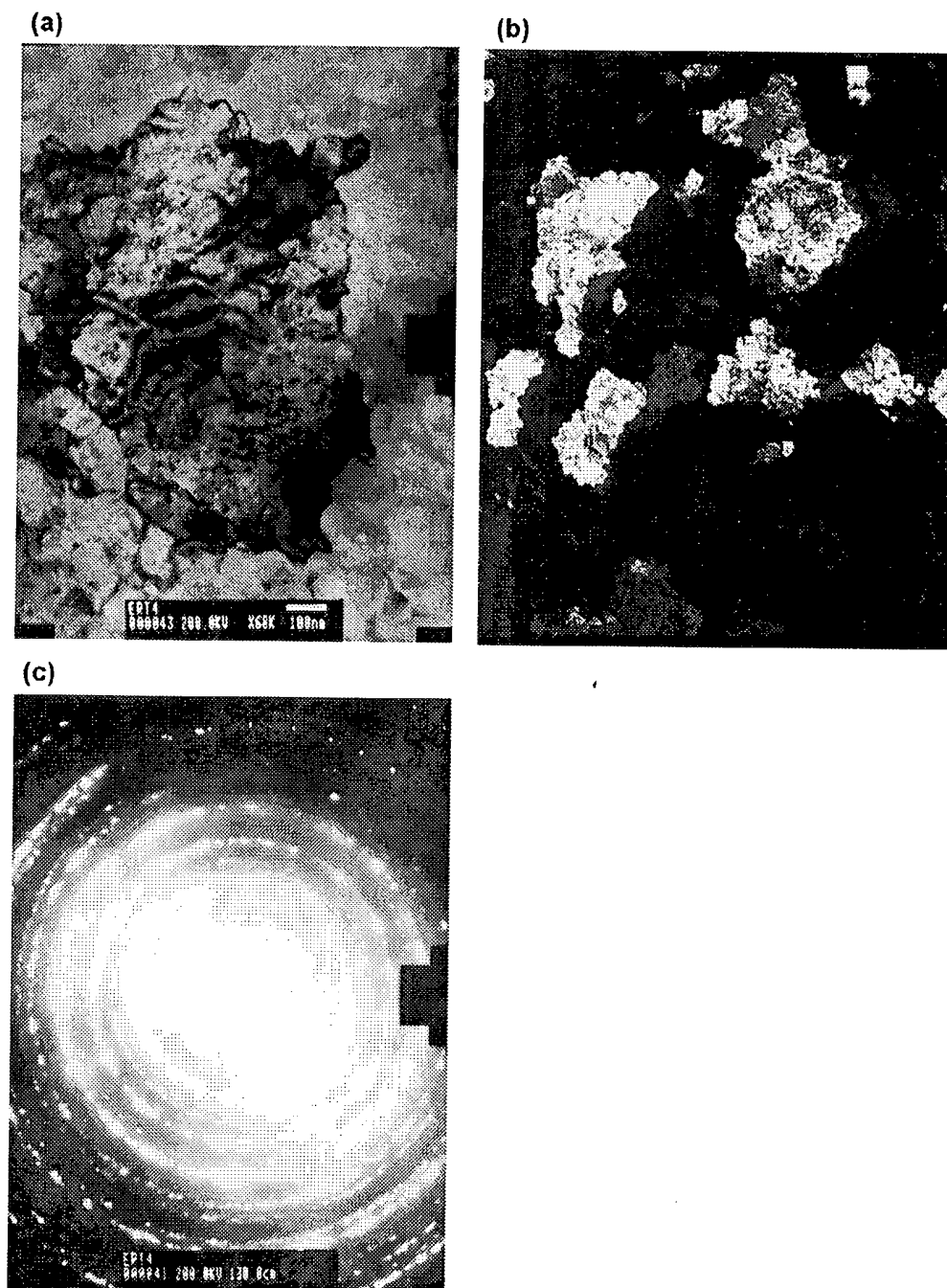


Fig. 15. TEM of the T sample showing presence of (a) subgrains and a large amount of strain fields; (b) darkfield image showing grain size of $1\text{ }\mu\text{m}$; (c) corresponding SADP.

sponds to a maximum temperature of 400°C were examined. The composition versus depth is given in Fig. 13. These results show that the Ni content decreases through the thickness corresponding to an increase in target temperature. The initial 0.1- μm thickness at the beginning of the deposition run shows a Ti composition of 45.0 at. % Ti, which is a fairly large deviation from the target composition. At the top, the film composition is closer to the composition of the target at 48.5 at. % Ti. This compositional gradation occurs over too large a thickness range 0.6 μm to be attributed to interfacial reactions, which have been shown to be only 10–100 nm in thickness [22].

3.4. Micrographs

Optical microscopy was used to observe the film attached to the substrate. After crystallization, the C samples were shiny, indicating a high modulus austenite phase, while T and H samples were cloudy (due to a highly textured surface) when cooled and shiny when heated up (Fig. 14). The surface texture is due to martensitic platelets that develop to accommodate the large residual tensile stresses in the film. Sputtered films typically have tensile residual stresses due to the more compact ordering of the film after crystallization compared with the initial amorphous phase. These martensitic platelets will disappear and reappear, corresponding to the change from austenite to martensite phase. This suggests and results confirm that at room

temperature the C samples are austenite and the T and H samples are martensite.

TEM samples were prepared by ion milling with a liquid nitrogen cold stage to prevent heating of the samples. Fig. 15 shows TEM micrographs of the T samples. Grain sizes were on the order of 1 μm . Higher magnification of individual grains showed the presence of subgrains within the larger grain. This and the straining of the lattice due to the martensitic structure explains why the XRD peaks of martensitic NiTi are so widely spread compared with typical XRD plots of other compounds. Subgrains have crystal planes oriented only a few degrees off from the other grains. A large number of these subgrains would spread the diffraction peaks over a wider angle in diffraction plots. The large amount of contrast within the grains indicate large amounts of strain fields due to either crystal defects or possible precipitates. These defects could have been introduced during the ion milling process. Twinning planes indicative of the martensitic phase was not observable. SADP (selective area diffraction pattern) of the T sample was inconclusive in determining the presence of the martensitic phase because the diffraction rings due to the (002), ($\bar{1}11$), (020), (111), and (012) planes of the monoclinic martensite phase were closely located within the highest intensity ring. However, the remaining rings were indexed as the B2 austenite structure. This implies that the film is multiphase. The presence of a multiphase across the area probably occurred after the ion milling.

Fig. 16 shows TEM micrographs of the C sample. Grain

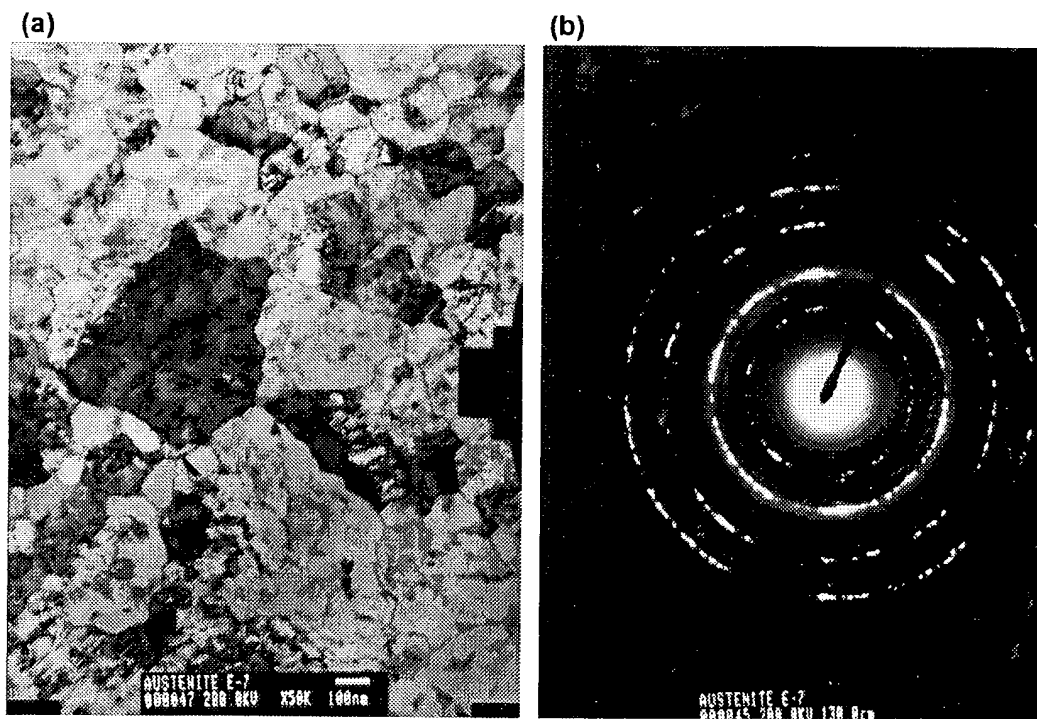


Fig. 16. (a) TEM of the C sample showing grains sizes on the order of 0.5 μm . (b) SADP indexed as the B2 austenite structure.

sizes were found to be on the order of $0.5\ \mu\text{m}$. The large contrast again indicates grains under large amounts of strain fields. SADP of the sample in Fig. 2b can be indexed as the austenite B2 cubic structure. The additional lower intensity diffraction rings could be due to oxides in the film.

TEM studies were done on the 600°C substrate heated sample to confirm the presence of precipitates. Fig. 17 shows the presence of intergranular precipitates. The precipitates were measured as $20\ \text{nm}$ in size. Grain sizes were similar to the previous samples varying from 0.2 to $1\ \mu\text{m}$ in

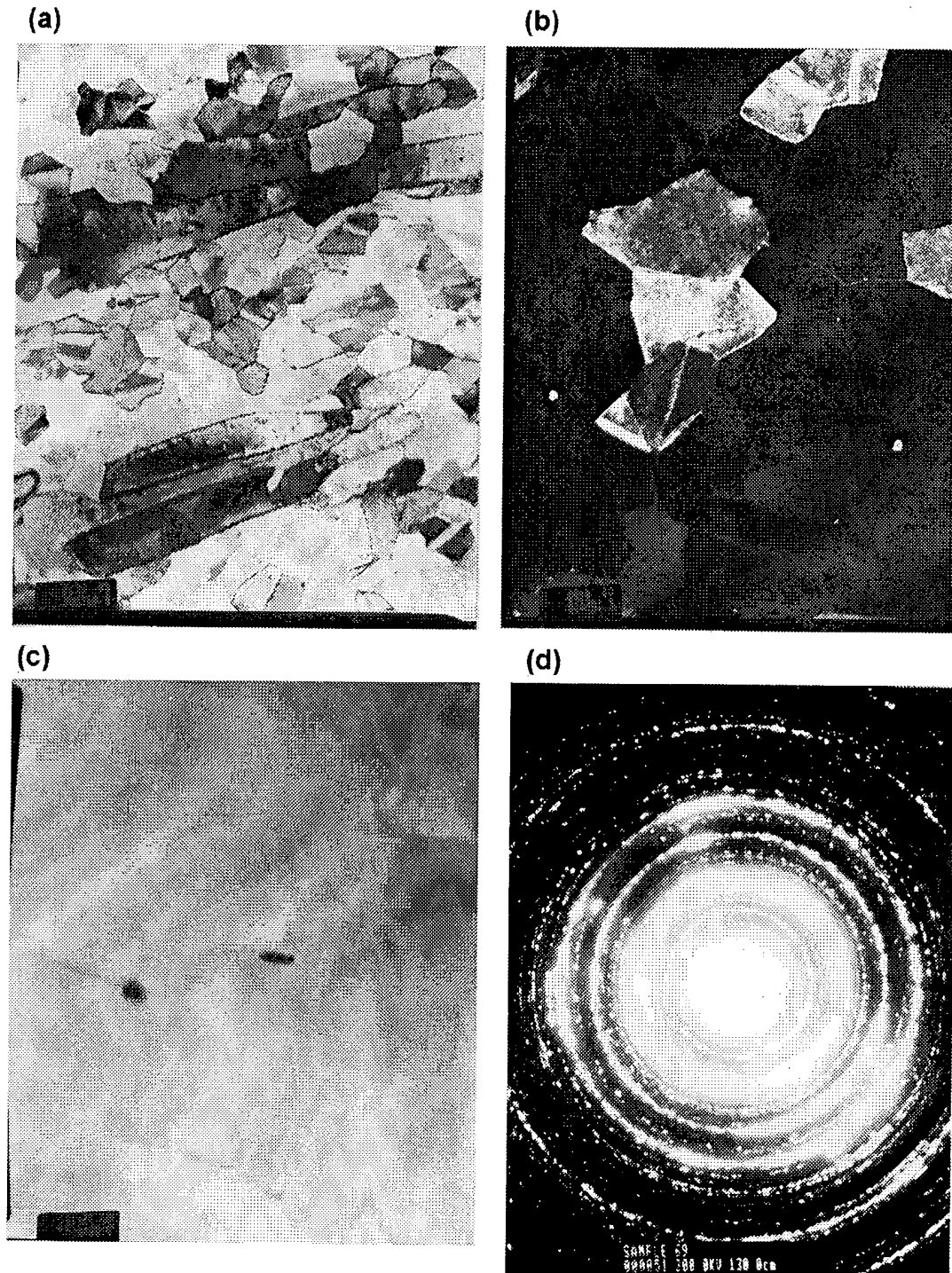


Fig. 17. TEM of the substrate-heated sample showing (a) grain sizes varying from 0.2 – $1\ \mu\text{m}$ with hardly any strain fields; (b) presence of intergranular precipitates; (c) precipitates of size on the order of $20\ \text{nm}$. (d) SADP of the sample.

size. The grains showed very little strain fields that was so predominant in the previous C and T samples. This is most likely due to the annealing effect of substrate heating. This suggest that the high residual stresses can be removed using substrate heating. SADP indicated again the presence of the B2 austenite phase. The numerous extra diffraction rings could not be indexed because of the large amount of possible oxides and precipitates that could have contributed to them.

4. Discussion

The two factors that could have influenced our results are substrate heating and target cleanliness. Addressing the first possibility, a red-hot target can radiatively heat the substrate

at close distances. XRD presented earlier showed that the films produced with substrate heating were austenite and not martensite at room temperatures. Thus, heating the substrate does not produce films with transformation temperature above 25°C.

The cleanliness of the target is another issue. Heating the target will degas any contaminants present on the surface. To evaluate this issue the cold target was presputtered for 2 h, a time sufficient to remove any surface contaminants and achieve stability in the relative sputtering yields of Ni and Ti. However, presputtering did not influence the material properties, therefore we conclude that presputtering did not affect the transformation temperatures of the C samples. In contrast, the initial T and H samples were presputtered for only 10 min with subsequent samples produced without presputtering. This is possible because the loadlock keeps the target under vacuum. Therefore, target cleanliness does not appear to have influenced our results.

The authors believe that the difference in film properties is due to target heating. A possible explanation for this phenomena follows. In sputtering the near equiatomic NiTi target, Ti has a higher sputtering yield. However, since conservation of mass demands that the flux of Ni and Ti from the target will be essentially equal, this causes an altered layer to exist on the target, about 800 Å thick, richer in Ni. The precise composition is such that both the difference in sputtering yield and an equal atomic flux of Ni and Ti are accommodated. However, even though the flux of Ni and Ti atoms from target is the same, films deposited by sputtering typically do not have the same composition as the target. This difference in film composition can be attributed to two factors: a difference in angular distribution of the sputtered species, and the sticking coefficient. It has been shown that the polar angular distribution of Ti is wider than that of Ni during sputtering [20,21]. This means that the Ti:Ni ratio is larger at low angles from the target surface plane and is smaller at 90° from the surface plane. Also, this difference in angular distribution will be more pronounced the further the substrate is from the target. We believe that the angular distribution is caused by the altered top layer of the target.

By heating the target to high temperatures, the binding energy decreases thereby changing the sputtering yields of Ni and Ti. This changes the composition of the altered layer. Diffusion also becomes a factor at high temperatures and also influences the composition of the altered layer. The altered layer is then changed by heating the target such

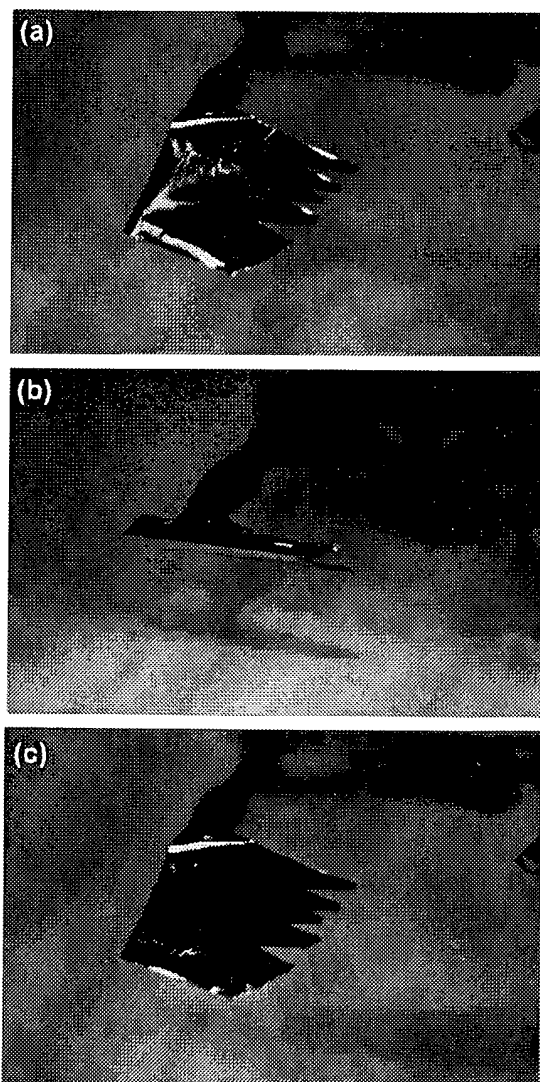


Fig. 18. Free-standing NiTi film exhibiting the two-way shape memory effect.

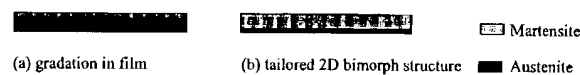


Fig. 19. (a) Gradation of a film due to gradual heating of the target accounting for the two-way SME. (b) More precise tailoring for a two-dimensional bimorph structure is possible, resulting in more defined layering of austenite and martensite.

that the difference in angular distribution of Ni and Ti becomes less pronounced resulting in a film composition closer to that of the target. Additional experimental tests will have to be done to detect this change in angular distribution.

The T-sample films also exhibit a two-way shape-memory effect intrinsic in the processing step, without further heat treatments. Fig. 18 shows the film at three stages: 25, 150, and back to 25°C. Without any external biasing the film initially flat, curled when heated and uncurled when cooled back to room temperature. We attribute this to the nonuniform properties across the film thickness. The gradation of properties is sufficient to produce the two-way SME. We hypothesize that the lower part of the film is austenite and the top part is martensite, possibly a superelastic system combined with a shape memory system (Fig. 19).

5. Conclusion

Sputter deposition of NiTi films exhibiting the SME above 25°C is difficult because of the sensitivity of the shape memory characteristics to composition. As a consequence sputter deposition from a single near equiatomic NiTi target typically requires compensation with titanium plates. In this paper we have shown that by heating the target to over 400°C during deposition, we can limit the loss of Ti and produce films exhibiting the SME above 25°C. Controlling the target temperature can also be used to produce films with the two-way SME. This novel method of fabricating NiTi films exhibiting the two-way effect can be improved with better process control, such that a precise two-dimensional austenite martensite bimorph structure can be tailored as desired.

Narrowing the compositional difference between the deposited film and the target by heating the target has tremendous implication in other fields of sputtering. For example, in deposition of magnetic alloys for the hard-drive industry a more uniform angular distribution of its constituents would result in a more compositionally uniform film that is closer in composition to that of the target. This would allow for much smaller magnetic domains thereby increasing the amount of data storage per unit area.

Acknowledgements

This work was partially sponsored by the Air Force Office of Scientific Research grant/contract number F49620-98-1-0058 managed by Brian Sanders.

References

- [1] J. Favalukis, A.S. Lavine, G.P. Carman, in: N.M. Wereley (Ed.), Proc. SPIE, Smart Structures and Materials 1999: Smart Structures and Integrated Systems, Newport Beach, CA, March 1–4, 1999, 3668 (1999) 617.
- [2] J.A. Walker, K.J. Gabriel, M. Mehregany, Sensors and Actuators A 21–23 (1990) 243.
- [3] J.D. Busch, A.D. Johnson, C.H. Lee, D.A. Stevenson, J. Appl. Phys. 68 (1990) 6224.
- [4] T.W. Duerig, K.N. Melton, D. Stockel, C.M. Wayman, Engineering Aspects of Shape Memory Alloys, Butterworth-Heinemann, London, 1990.
- [5] S. Miyazaki, K. Nomura, in: T. Higuchi, K. Ikuta (Eds.), Proc. SPIE, Micro Electro Mechanical Systems: An Investigation of Micro Structures, Sensors, Actuators, Machines and Robotic Systems, Oiso, Japan, Jan. 25–28, 1994, (1994) 176.
- [6] R.H. Wolf, A.H. Heuer, J. Microelectromech. Syst. 4 (1995) 206.
- [7] A. Gyobu, Y. Kawamura, H. Horikawa, T. Saburi, Mater. Trans. JIM 37 (1996) 697.
- [8] E. Quandt, C. Halene, H. Holleck, K. Feit, M. Kohl, P. Schlomacher, A. Skokan, Sensors and Actuators A 53 (1996) 434.
- [9] P. Krut'evich, A.P. Lee, P.B. Ramsey, J.C. Trevino, J. Hamilton, M.A. Northrup, J. Microelectromech. Syst. 5 (1996) 270.
- [10] K. Kuribayashi, T. Taniguchi, M. Yositate, S. Ogawa, in: A.P. Jardine, G.C. Johnson, A. Crowson, M. Allen (Eds.), Smart Materials Fabrication and Materials for Micro-Electro-Mechanical Systems, San Francisco, CA, April 28–30, 1992, MRS (1992) 167.
- [11] K. Kuribayashi, S. Shimizu, T. Nishinohara, T. Taniguchi, Proc. Int. Conf. On Intelligent Robots and Systems, 1993, p. 1697.
- [12] J.D. Busch, M.H. Berkson, A.D. Johnson, in: M. Chen, M.O. Thompson, R.B. Schwarz, M. Libera (Eds.), Phase Transformation Kinetics in Thin Films Symposium, Anaheim, CA, USA, 29 April–1 May, 1991, MRS (1991) 91.
- [13] D.S. Grummon, T.J. Pence, in: E.P. George, R. Gotthardt, K. Otsuka, S. Troler-McKinstry, M. Wun-Fogle (Eds.), Materials for Smart Systems II. Symposium, Boston, MA, Dec. 2–5, 1996, MRS (1997) 331.
- [14] Q. Su, S.Z. Hua, M. Wuttig, J. Alloys, Compounds 211 (1994) 460.
- [15] S. Miyazaki, T. Hashinaga, K. Yumikura, H. Horikawa, T. Ueki, A. Ishida, in: A.P. Jardine (Ed.), Smart Structures and Materials 1995, Smart Materials, San Diego, CA, Feb. 27–28, 1995, SPIE ISOE (1995) 156.
- [16] A. Ishida, A. Takei, M. Sato, S. Miyazaki, in: E.P. George, S. Takahashi, S. Troler-McKinstry, K. Uchino, M. Wun-Fogle (Eds.), Materials for Smart Systems Symposium, Boston, MA, Nov. 28–30, 1994, MRS (1995) 381.
- [17] C.A. Ray, C.L. Sloan, A.D. Johnson, J.D. Busch, B.R. Petty, in: A.P. Jardine, G.C. Johnson, A. Crowson, M. Allen (Eds.), Smart Materials Fabrication and Materials for Micro-Electro-Mechanical Systems, San Francisco, CA, April 28–30, 1992, MRS (1992) 161.
- [18] W.L. Benard, H. Kahn, A.H. Heuer, M.A. Huff, J. Microelectromech. Syst. 7 (1998) 245.
- [19] L.G. Carpenter, Vacuum Technology: An Introduction, 2nd ed., Adam Hilger, Bristol, 1982.
- [20] V.S. Chernysh, V.S. Tuboltsev, V.S. Kulikauskas, Nucl. Instrum. Methods Phys. Res. B 140 (1998) 303.
- [21] I. Neshev, R.G. Vichev, S. Tzanev, S.S. Todorov, Vacuum 44 (1993) 209.
- [22] Q. Su, S.Z. Hua, M. Wuttig, in: V.K. Varadan (Ed.), Smart Structures and Materials 1994, Smart Materials, Orlando, FL, Feb. 14–16, 1994, Proc. SPIE 2189 (1994) 409.

[Previous
Article](#)

[Next
Article](#)

[Back to
Table of
Contents](#)

[Back to
the Issues
List](#)

[Back to
the
Journal
Index](#)

[Search](#)

Thin Solid Films, Vol: 370, Issue: 1-2, pp. 18-29, July 17, 2000

Title:

Sputter deposition of NiTi thin film shape memory alloy using a heated target

Authors:

Ho, Ken K.^a; Carman, Gregory P.^a

Affiliations:

a. Mechanical and Aerospace Engineering, University of California, Los Angeles,
38-137m Engineering IV, 420 Westwood Plaza, Los Angeles, CA 90095-1597,
USA

Address:

(No address specified)

Keywords:

Deposition process; NiTi; Shape memory alloy; Sputtering

Abstract (English):

In this paper we present a novel method for depositing NiTi thin film by DC sputtering. The film has transformation temperatures very close to that of the target. The new process involves heating the target and does not require compositional modification of the NiTi target. Results from X-ray diffraction, differential scanning calorimeter, four-point probe, Rutherford backscattering, and transmission electron microscopy are presented. These results indicate that compositional modification can be produced by varying the target temperature. Films produced from hot targets have compositions similar to the target while films produced from cold targets were Ti deficient. Films that were produced by gradual heating of the target have compositional gradation through the film thickness. The graded films exhibit the two-way shape memory effect.

Publisher:

Elsevier Science

Language of Publication:

English

Item Identifier:

S0040-6090(00)00947-0

Publication Type:

Full Length Article

ISSN:

0040-6090

This journal article is available on-line in the following forms:

- [Article Full-text PDF \(2.86 MB\)](#)
- [Get article citation \(Refer format\)](#)